8.1 OBJECT KINETIC MONTE CARLO SIMULATIONS OF RADIATION DAMAGE IN TUNGSTEN SUBJECTED TO NEUTRON FLUX WITH PKA SPECTRUM CORRESPONDING TO HFIR —

G. Nandipati, W. Setyawan, H. L. Heinisch, K. J. Roche, R. J. Kurtz (Pacific Northwest National Laboratory) and B. D. Wirth (University of Tennessee)

OBJECTIVE

The objective of this work is to study the damage accumulation in pure tungsten (W) subjected to a neutron flux with a primary knock-on atom (PKA) spectrum corresponding to the high flux isotope reactor (HFIR), using the object kinetic Monte Carlo (OKMC) method.

SUMMARY

We used our recently developed lattice based object kinetic Monte Carlo (OKMC) code, *KSOME* [1], to carry out simulations of radiation damage in bulk W. In this report, we present preliminary results of our study of, the effect of the maximum size of self-interstitial atom (SIA) clusters allowed to rotate on the defect accumulation in bulk tungsten with 1µm grain size when subjected to neutron flux having PKA spectrum corresponding to HFIR at 1025 K for the dose rates in the range 0.17 x 10^{-4} to 0.17 x 10^{-8} dpa/s.

PROGRESS AND STATUS

Results

A complete description of the simulation parameters used and how the present simulations are preformed is available in Ref. [2]. Figure 1 (a-f) shows a comparison of the number density of vacancies and vacancy clusters, and average vacancy cluster diameters as a function of dose at dose rates of 0.17 x 10^{-4} to 0.17 x 10^{-8} dpa/s, when SIA clusters up to size 5 (Case1, left column) and up to size 10 (Case 2, right column) are allowed to rotate. Figure 2 shows a comparison of the vacancy microstructures at various dose rates at 1.0 dpa for both cases. Due to lack of space, only the order of the magnitude of the dose rates is shown in both figures, while the factor of 0.17 is omitted, a value of 10^{-4} dpa/s in a figure represents a dose rate of 0.17 × 10^{-4} dpa/s. Note that in these simulations the effect of both intragranular defects and transmutation are ignored.

As expected the number density of vacancies and vacancy clusters, and the average size of vacancy clusters decrease when the maximum allowed size of the rotation of SIA clusters is increased, and this is due to the increase in the number of recombinations. The general behavior of the number density of vacancies and their clusters, and the average vacancy cluster size with dose rates in both cases remains the same, but the behavior is different as a function of dose, especially, at the dose rates of 0.17 x 10^{-4} and 0.17 x 10^{-5} dpa/s for *case-II*. In the latter case, the vacancy cluster size appears to have saturated at 1.05 nm, while the number density of vacancies and vacancy clusters increases very slowly with dose. For lower dose rates, although the number density of vacancies increases much more slowly in *case-II*, it shows similar behavior with dose for both the cases.

In both cases void lattice formation was observed for dose rates from 0.17 x 10^{-6} to 0.17 x 10^{-8} dpa/s (See Figure 2 (e-h)), while for the dose rates of 0.17 x 10^{-4} and 0.17 x 10^{-5} dpa/s void lattice formation was observed for case-I but not for *case-II*. At these dose rates, even though the density of vacancy clusters is higher than at lower dose rates, the spatial distribution of vacancy clusters appears to be random. This could be due to the fact that the sizes of the vacancy clusters are very small and they appear to have saturated at 1.05 nm (see Figure 1(f)). This suggests that for the dose rates of 0.17 x 10^{-4} and 0.17 x 10^{-5} dpa/s for *case-II*, either the formation of large vacancy clusters is very slow or they do not survive long enough to grow beyond an average size of 1.05 nm.

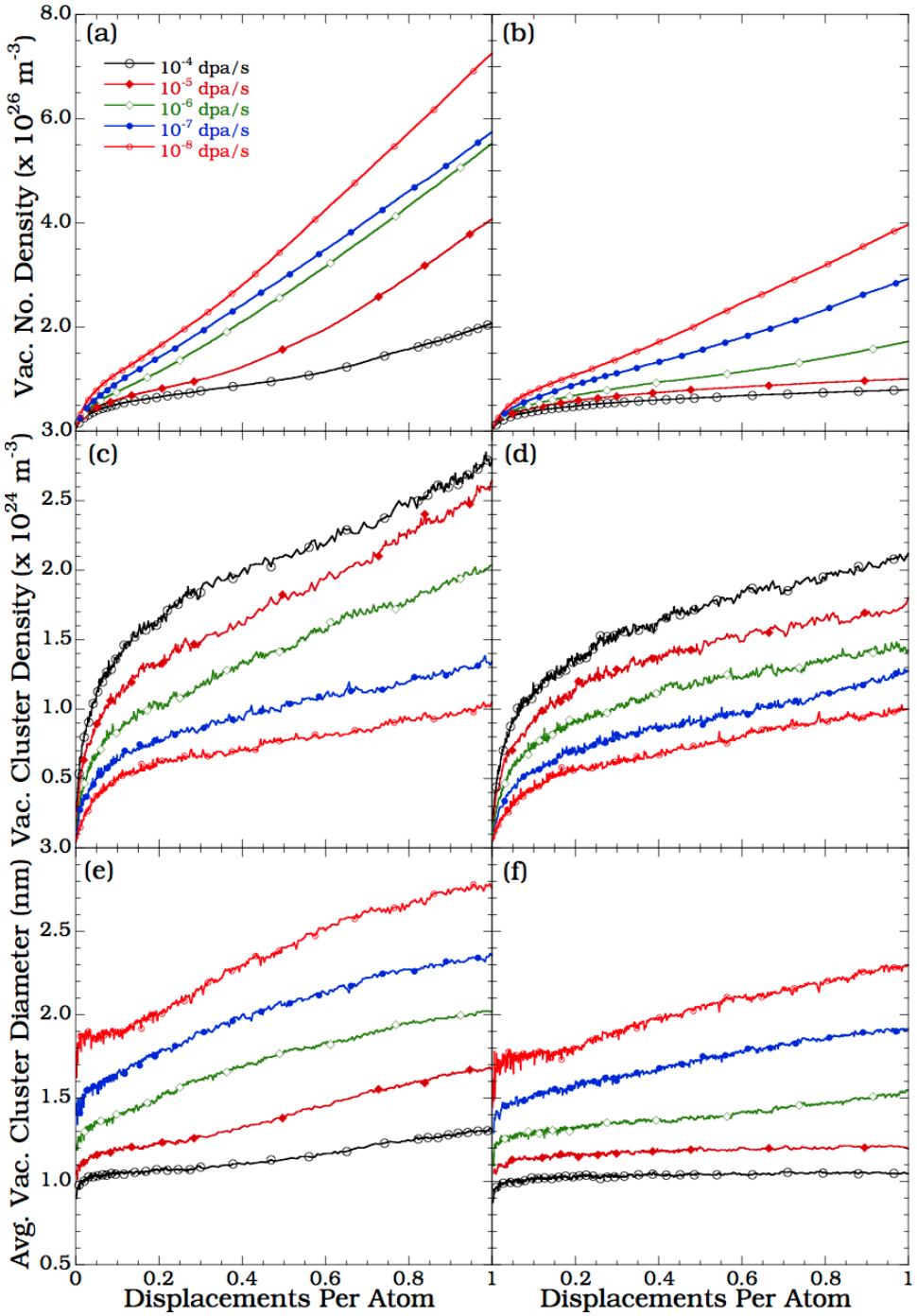

Figure 1. Comparison of (a-b) vacancy number density and (c-d) vacancy cluster density and (e-f) average vacancy clusters size at various dose rate when SIA clusters are allowed to rotate up to size of 5 (left column) and 10 (right column).

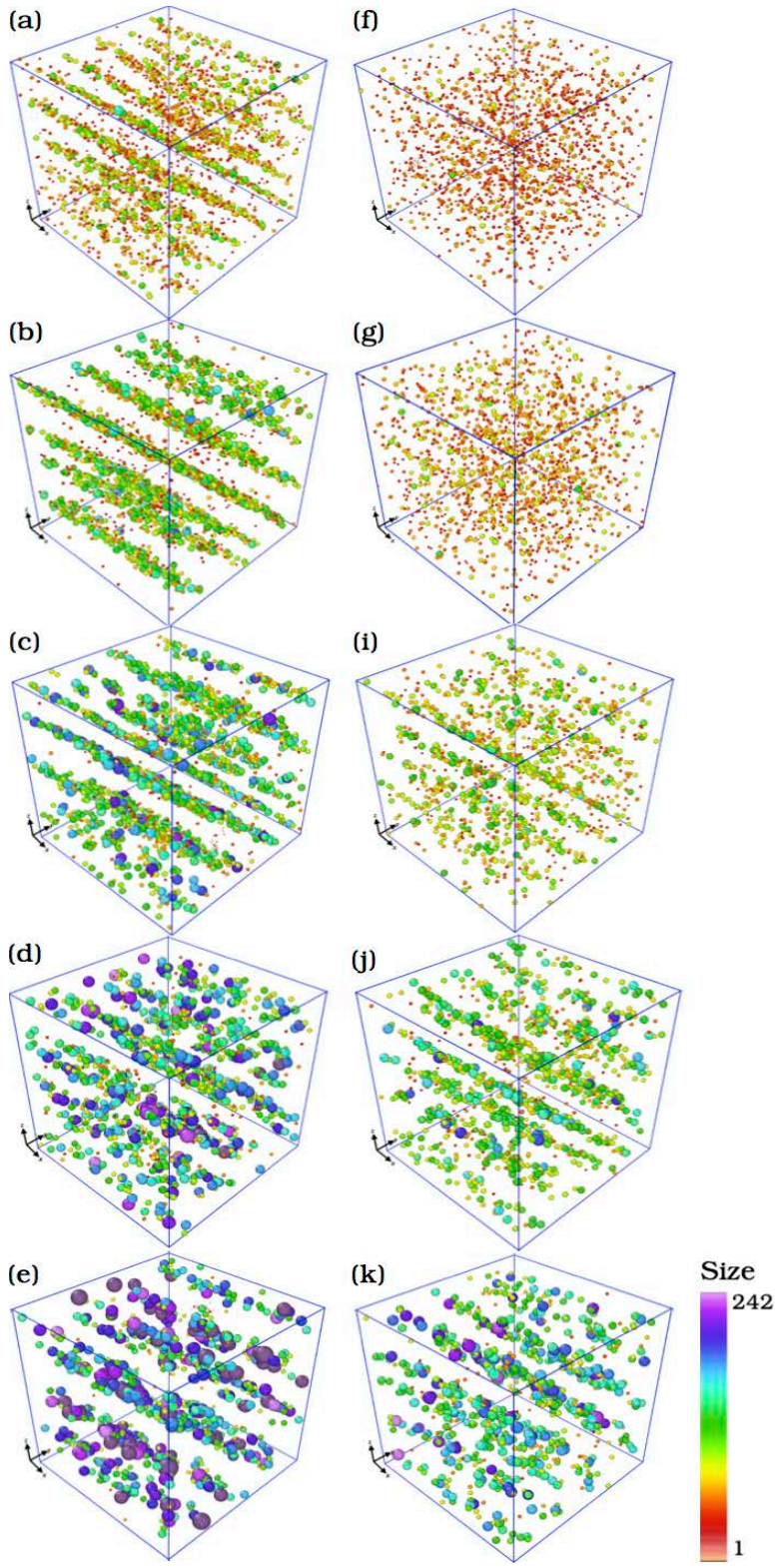

Figure 2. Snap shots of vacancy cluster microstructure at a dose of 1dpa when SIA clusters up to size (a-e) 10 (g-k) 5 at dose rates of (a, g) 10^{-4} (b, h) 10^{-5} (c, i) 10^{-6} (d, j) 10^{-7} (e, k)10^{-8} dpa/s.

Future Work

We will carry out further analysis of available data and also carry out additional simulations to understand defect accumulation at various dose rates, PKA energies, temperatures, simulation cell and grain size, and also at different PKA spectrums.

Acknowledgement

All computations were performed partly on HOPPER at National Energy Research Scientific Computing Center (NERSC) and PNNL's institutional computing (PIC) systems.

References

[1] G. Nandipati *et al* Semiannual Progress Report DOE/ER-0313/54, Jun 2013,179-183.
[2] G. Nandipati *et al* http://arxiv.org/pdf/1510.02732.pdf.